Supporting Information

Steering CO resistance and Catalytic Activity of PtRu Alloy in Methanol Oxidation with Atomically Dispersed Ni

Guoqing Zhang[1#], Jiankun Li[1#], Shiyi Li[1], Yixing Wang[1, 2], Linfeng Lei[1, 2], Minghui Zhu[1], Linzhou Zhuang[1], Zhi Xu[1]*

[1]State Key Laboratory of Chemical Engineering, School of Chemical Engineering, East China University of Science and Technology, Shanghai, 200237, China

[2]Suzhou Laboratory, Suzhou, 215000, China

[#]These authors contributed equally

Corresponding Email: lzzhuang@ecust.edu.cn (L. Zhuang)

Chemicals and Materials

Chloroplatinic acid hexahydrate ($H_2PtCl_6 \cdot 6H_2O$, AR) was purchased from Aladdin Industrial Inc. (Shanghai, China). Ruthenium chloride hydrate ($RuCl_3$ xH_2O) was purchased from Shanghai Titan Scientific Co., Ltd. Anhydrous Nickel (II) chloride (Nickel (II) Chloride, Anhydrous) was purchased from Beijing InnoChem Science & Technology Co., Ltd. Methanol, ethanol, acetone, hydrochloric acid (HCl, 37%) and sulfuric acid (H_2SO_4, 98%) were supplied by Sinopharm Chemical Reagent Co. Ltd. (Shanghai, China). Commercial Pt/C catalyst (Pt/C, 20wt%) was supplied by Johnson-Matthey Corp. Nafion solution (5 wt.%) were bought from Alfa Aesar. All chemicals were used as received without further purification, and all solutions were freshly prepared with ultrapure water (18.2 MΩ cm^{-1}).

Synthesis of catalysts

Before electrodeposition, the SS (15 mm × 10 mm × 0.3 mm) was ultrasonically placed in acetone and 10wt% HCl solution for 30 min to remove the residual organic matter and oxide impurities. Then, the processed SS was immersed in anhydrous ethanol for later use after washing with deionized water thrice. All electrocatalysts were prepared via galvanostatic electrodeposition using a three-electrode system on Auto lab (Metrohm, Multi Autolan m204) electrochemical workstation. SS, a platinum sheet (Pt sheet) (10 mm × 10 mm× 3 mm), and $HgSO_4$ (0.652 V vs. RHE, saturated K_2SO_4) were used as the working electrode (WE), counter electrode (CE), and reference electrode (RE), respectively. The composition of the electrolyte and the electroplating parameters are shown in Table S1. Before the preparation process, the pH of the electrolyte was adjusted to 1.5 using a 0.5 M H_2SO_4 solution. After electroplating, the working electrode was rinsed three times alternately with deionized water and anhydrous ethanol, and then dried before testing.

As a control, 12.5 mg of 40 wt% commercial Pt/C powder and 50 μL of 5 wt% Nafion were added to 950 μL of isopropanol. The mixture was then ultrasonically dispersed for 1 hour to obtain a uniform ink. 5 μL of catalyst ink was doped onto the glass carbon electrode(GCE, 5 mm of diameter, 0.196 cm^{-2}) and dried in air

atmosphere for 30 min to make the work electrode.。

Characterizations

Morphologies of the as-synthesized PtRu/SS and PtRuNi/SS nanocomposites were examined on a JEM-2100 Plus transmission electron microscope (TEM), which was operated at 200 kV (and the particle size was measured using Nano Measure 1.2 software). Scanning electron microscopy (SEM) images were collected using a ZEISS Gemini 300. Specimens were prepared by ultrasonically suspending the particles in deionized water. Drops of such suspensions were deposited onto a standard Cu grid covered with carbon film (200 mesh) and allowed to dry before being inserted into the microscope. X-ray Diffraction (XRD) patterns reveal the bulk structure of the catalyst. XRD data was collected on a Bruker D8 Advance X-ray Polycrystalline Diffractometer at 40 kV/40 mA with Cu Ka radiation (k = 1.541874 Å) in the angular range of 30~80° for the 2θ angle. X-ray photoelectron spectroscopy (XPS) tests were conducted with Thermo Scientific Escalab 250Xi. All binding energies were referenced to the C 1s line at 284.8 eV from adventitious carbon. The average chemical compositions of catalysts were determined using an IRIS advantage inductively coupled plasma atomic emission spectroscopy (ICP-AES) system (Thermo, USA).

Electrochemical measurements

All the electrochemical measurements were conducted on an Auto Lab (Metrohm，Multi Autolan m204) electrochemical workstation with a typical three-electrode configuration. All the recorded potentials were converted to the reversible hydrogen electrode (RHE) according to the follow formula: $E_{vs.\ RHE} = E_{vs.\ MSE} + 0.059*pH + 0.652$

Cyclic voltammograms (CVs) were recorded at room temperature with a scan rate of 50 mV/s in N_2-saturated 0.5 M H_2SO_4 solution. The electrochemical surface area (ECSA) was calculated by both integrating charge from the hydrogen adsorption/desorption (ECSA-H). For ECSA-H calculation, CV recorded in N_2-saturated 0.5 M H_2SO_4 solution was used with applying the following equation:

$$ECSA = \frac{Q_H}{m * q}$$

where Q_H represents the surface charge for hydrogen desorption, q represents the charge required for the adsorption/desorption of hydrogen of a monolayer of Pt (210 μC cm^{-2}) and m is the Pt loading amount.

The MOR/EOR curves were recorded in N_2-saturated 0.5 M H_2SO_4 solution containing 1 M methanol/ethanol between 0~1.25 V (vs RHE). The corresponding MOR/EOR stability tests were carried out *via* chronoamperometric (CA) tests at a fixed potential of 0.75 V (vs. RHE).

CO stripping curves were recorded in 0.5 M H_2SO_4 electrolyte. Firstly, the working electrode was held at a constant potential of 0.1 V (vs. RHE) in CO-saturated 0.5 M H_2SO_4 solution for 20 minutes. Then, N_2 was bubbled into the electrolyte for 20 min to remove CO gases. Finally, the CO stripping curves were recorded between 0 V and 1.25 V (vs RHE).

Electrochemical in situ attenuated total reflection infrared (ATR-IR) spectroscopy

Surface-enhanced In situ ATR-IR (SEIRAS) was measured at PerkinElmer spectrum 100 spectrometer equipped with a mercury cadmium telluride (MCT) detector, a variable angle specular reflectance (Jiaxing Puxiang Tech. Ltd,) and cell (Jiaxing Puxiang Tech. Ltd,) including a Pt CE, an Ag/AgCl RE, a gas inlet port and a gas outlet port. As the WE, SS supported catalyst was tightly contacting the surface of the silica prism. Before electrochemical measurements, the electrolyte (1 M MeOH, 0.5 M H_2SO_4) was injected into the cell. A CH1242C potentiostat was employed to record the electrochemical response. The spectrum was collected step-wisely from 0.10 V to 1.2 V vs. RHE with a dwell time of 2 min at each potential.

Density functional theory (DFT) calculations

All DFT calculations were conducted by using the Vienna *Ab initio* Simulation Program (VASP),[1] and the projector-augmented plane wave (PAW) pseudopotentials were used for the elements involved with a cut-off energy of 450 eV.[2] The generalized gradient approximation (GGA) of Perdew-Bruke-Ernzerhof (PBE) was used to treat the exchange-correlation of electrons.[3] Smearing (0.2 eV) based on the

method of Methdessel-Paxton[4] was applied in the total energy calculations. The convergence threshold for ionic steps in geometry optimization was 1×10^{-5} eV. Geometries were deemed converged when the forces on each atom were below 0.02 eV $Å^{-1}$. s. The Brillouin zone was sampled using a (3×3×1) Γ-centered mesh. The van der Waals corrections are applied to all the calculations as implemented in the DFT-D3 method due to its good description of long-range vdW interactions.[5] Given the presence of water, chich can affect the energetics of different electrochemical systems, polarizable implicit solvent models were calculated using VASPsol.[6] Pt(111), PtRu(111) facets were selected for calculations in this study according to TEM results and previous reports.[7] PtRuNi(111) was constructed by replacing a Ru atom in the first layer with Ni. The Ru sites in three slabs are fully covered by OH groups in the electrode potential range $0.5 < V < 0.75V$ according to previous studies.[8] A vacuum region larger than 15 Å was applied along the direction normal to the slab plane to avoid the interaction between periodic supercells. To effectively reduce the computational cost, the bottom two layers were fixed and the top two layers were allowed to relax in this work, which has been proved to be enough accurate for convergence with respect to the adsorption energies in previous works.[9]

The methanol electrooxidation reaction pathway was considered in a continuous dehydrogenation process:

$$* + CH_3OH(l) \rightleftharpoons *CH_3OH \quad (1)$$

$$*CH_3OH \rightleftharpoons *CH_2OH + H^+ + e^- \quad (2)$$

$$*CH_2OH \rightleftharpoons *HCOH + H^+ + e^- \quad (3)$$

$$*HCOH \rightleftharpoons *HCO + H^+ + e^- \quad (4)$$

$$*HCO \rightleftharpoons *CO + H^+ + e^- \quad (5)$$

$$*CO + H_2O \rightleftharpoons *COOH + H^+ + e^- \quad (6)$$

$$*COOH \rightleftharpoons *CO_2 + H^+ + e^- \quad (7)$$

$$*CO_2 \rightleftharpoons CO_2(g) + H^+ + e^- \quad (8)$$

where * represents an active site on the catalysts surface. The Gibbs free energy of adsorbates and non-adsorbed gas phase molecules can be obtained by the following expression [10]:

$$G(T) = E_{DFT} + G_{correct}(T) = E_{DFT} + ZPE - TS + \Delta U_{0\rightarrow T} \quad (9)$$

where $G(T)$ is the Gibbs free energy at temperature T, E_{DFT} is the DFT energy,

$G_{\text{correct}}(T)$ is the thermal correction to Gibbs free energy, and ZPE, S, $\Delta U_{0\rightarrow T}$ are the zero−point energy, entropy and internal energy change induced by temperature, respectively. The $G_{correct}(T)$ was caculated using the VASPKIT tool.[11] T is the temperature (T = 298.15 K).

Free-energy changes for each electrochemical step involving a proton and electron transfer were computed based on the computational hydrogen electrode model proposed by Nørskov et al.56, in which the free energy (G) of $H^+ + e^-$ is equal to $1/2H_2(g)$, which corresponds to the RHE. Therefore, in the RHE, the chemical potential of a proton−electron pair is defined as $G\,(H^+ + e^-) = 1/2G(H_2) - eU$

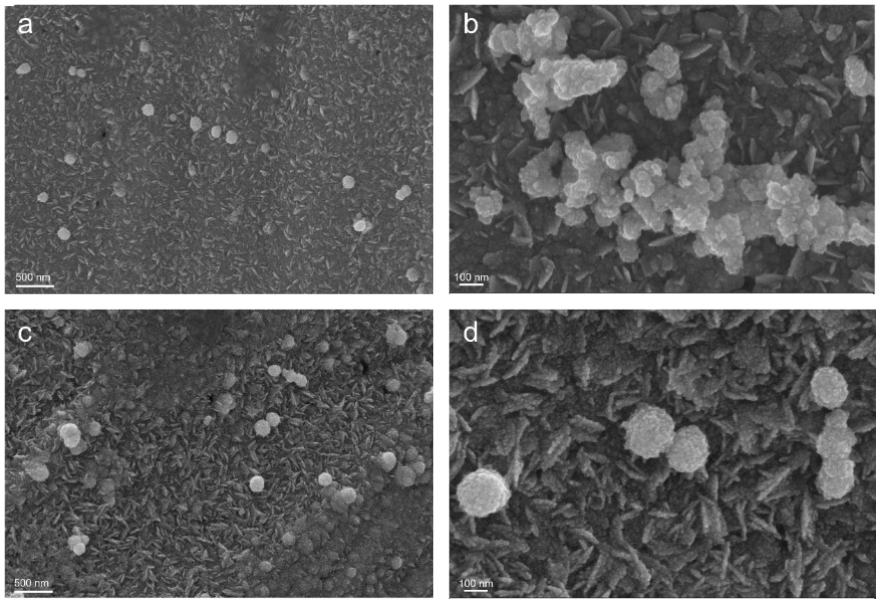

Fig. S1 Representative SEM images of a) and b) PtRuNi/SS, c) and d) PtRu/SS.

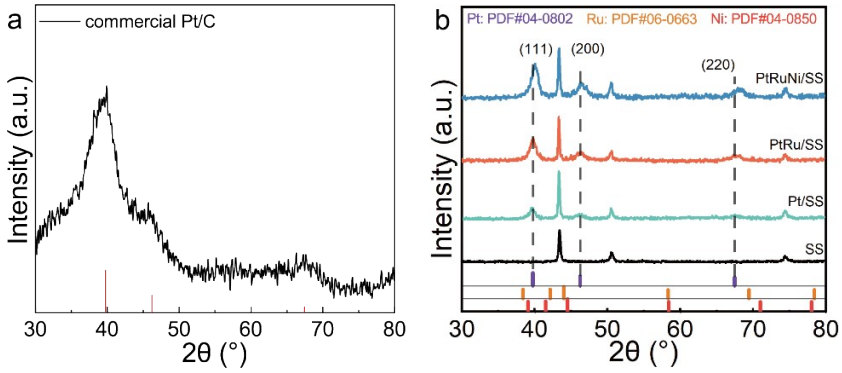

Fig. S2 XRD patterns a) commercial Pt/C and b) stain steel and different catalysts.

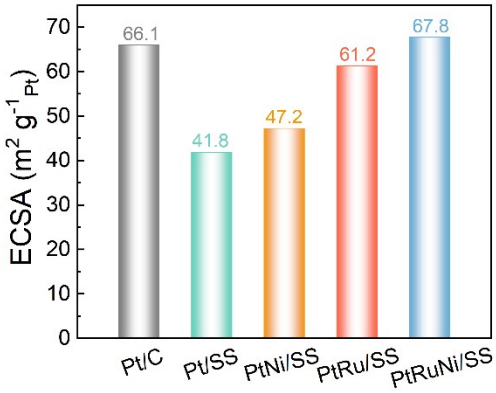

Fig. S3 ECSA-normalized peak current density of different catalysts.

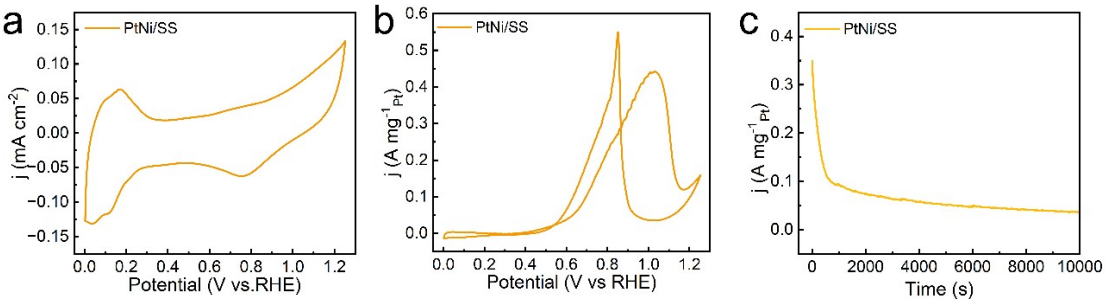

Fig. S4 Electrochemical performance of PtNi/SS for MOR. a) The CV curves were tested in the N_2-saturated 0.5 M H_2SO_4, b) 0.5 M H_2SO_4 and 1 M CH_3OH and c) CA tests of PtNi/SS.

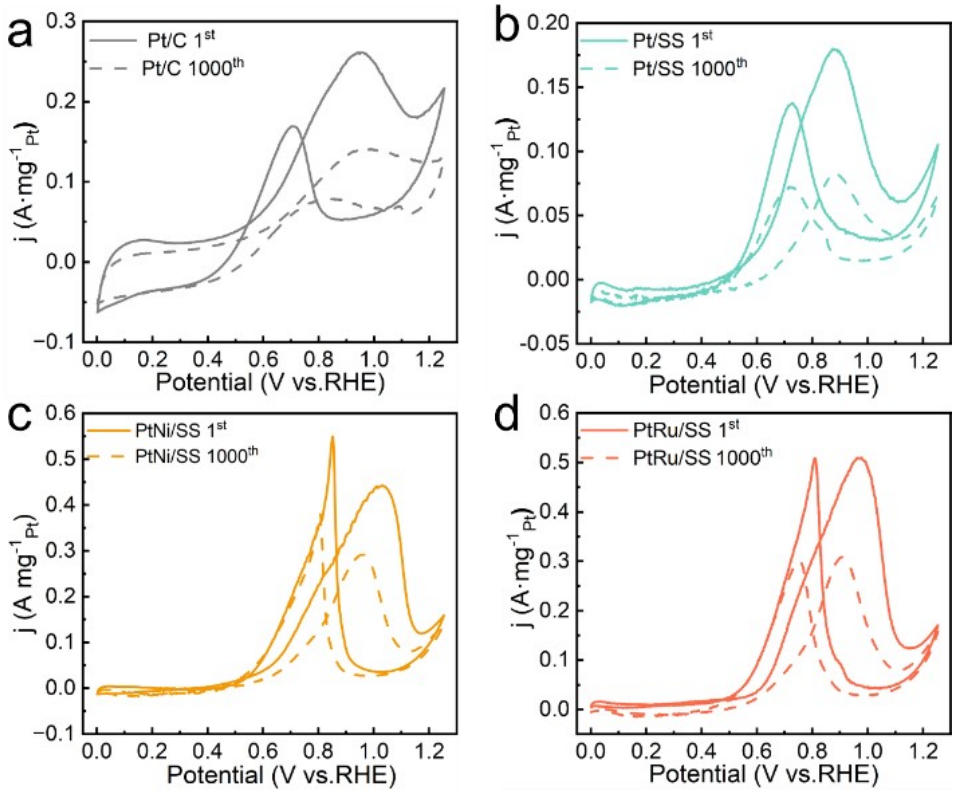

Fig. S5 Pt mass-normalized MOR curves of a) commercial Pt/C, b) Pt/SS, c) PtNi/SS and PtRu/SS before and after stability tests.

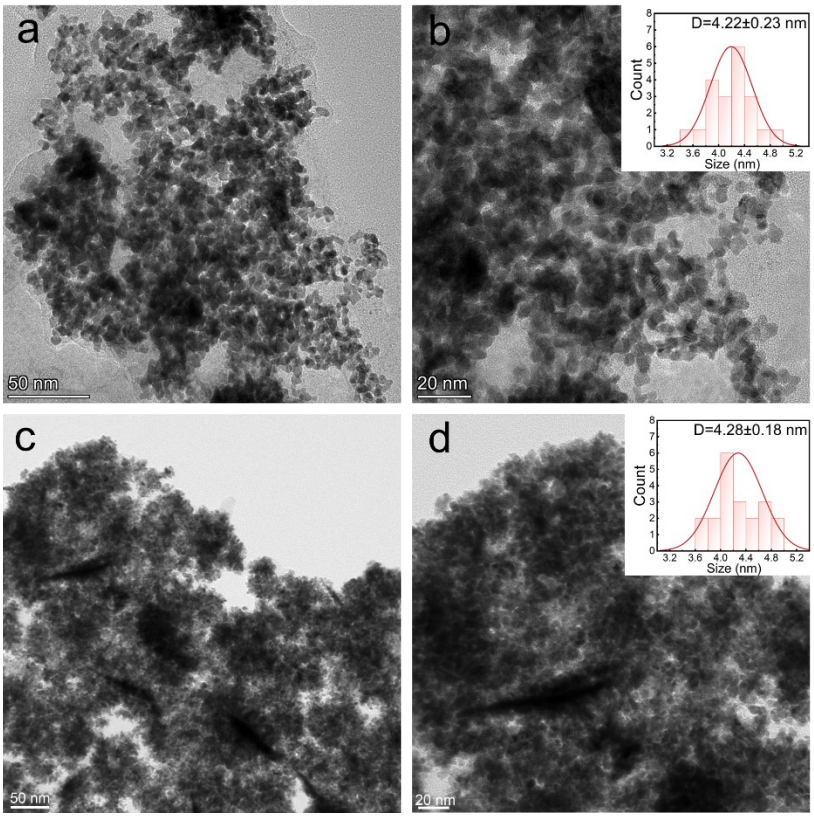

Fig. S6 Representative TEM images of PtRuNi. a) and b) before ADT tests. c) and d) after ADT tests.

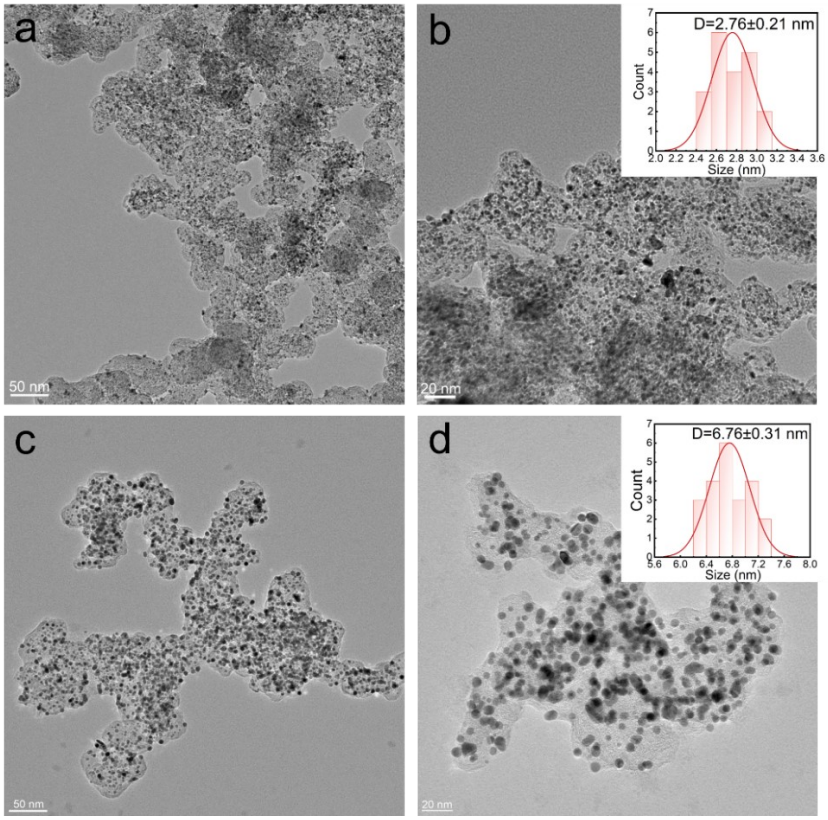

Fig. S7 Representative TEM images of commercial Pt/C a) and b) before ADT tests. c) and d) after ADT tests.

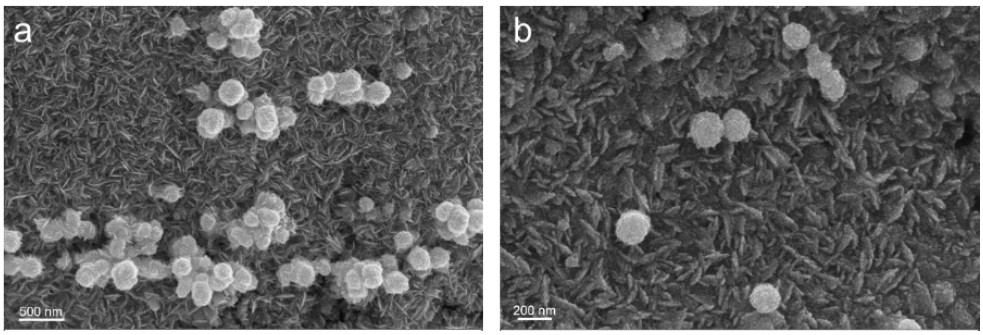

Fig. S8 Representative SEM images of PtRuNi after long-term MOR tests.

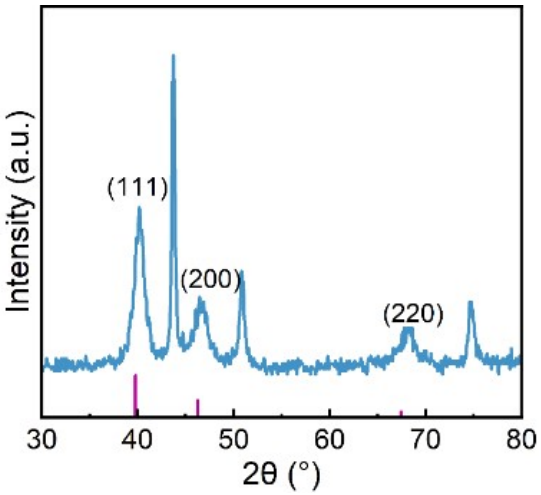

Fig. S9 XRD pattern of PtRuNi/SS after long-term MOR tests.

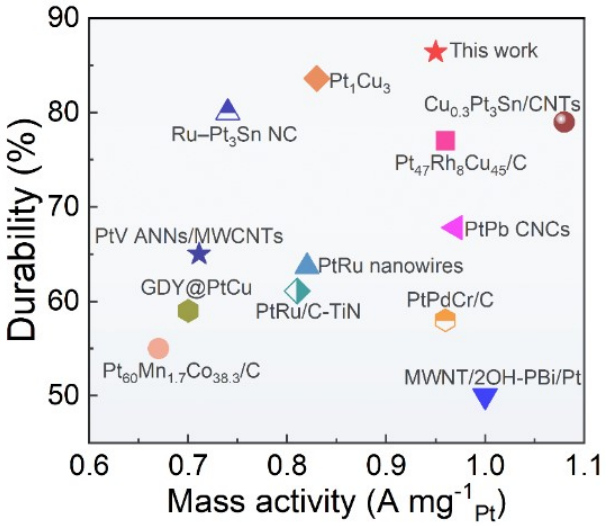

Fig. S10 Comparisons of MOR activities of PtRuNi/SS to reported Pt-based catalysts. The corresponding values and references are specified in Table S3.

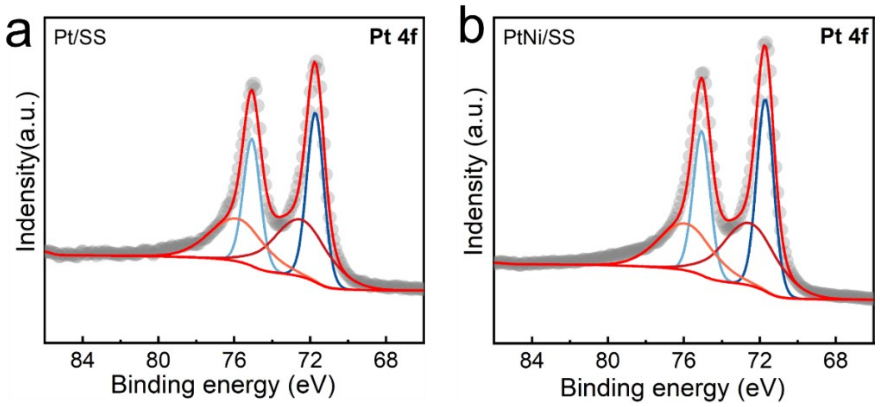

Fig. S11 High-resolution Pt *4f* XPS spectra of a) Pt/SS and b) PtNi/SS

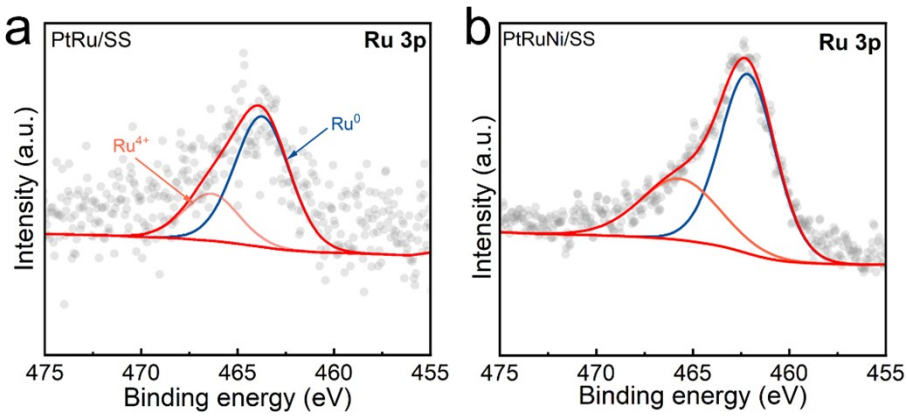

Fig. S12 High-resolution Ru *3p* XPS spectra of a) PtRu/SS and b) PtRuNi/SS.

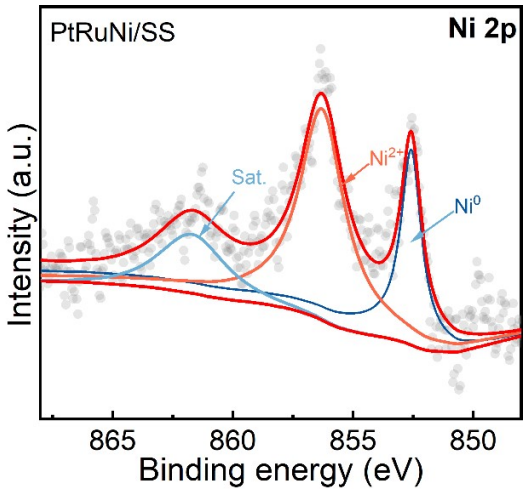

Fig. S13 High-resolution Ni *2p* XPS spectra PtRuNi/SS.

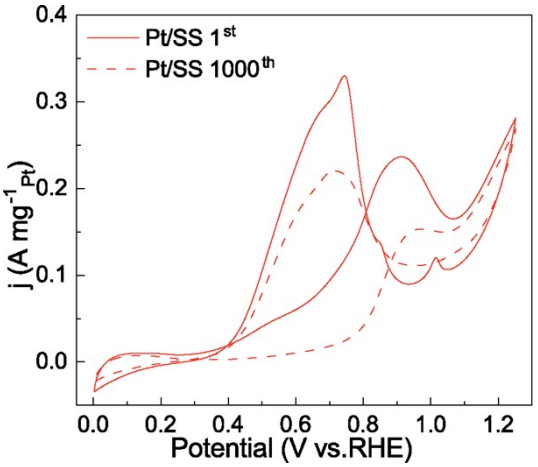

Fig. S14 Pt mass-normalized EOR curves of Pt/SS before and after stability tests.

Table S1. Synthesis conditions table

	PtRuNi/SS	PtRu/SS	PtNi/SS	Pt/SS
$H_2PtCl_6 \cdot 6H_2O$ (mg)	10.00	10.00	10.00	10.00
$RuCl_3 \cdot xH_2O$ (mg)	5.18	5.18	0	0
$NiCl_2$ (mg)	259.60	0	259.60	0
Current density ($mA \cdot cm^{-2}$)	50	50	50	50
Time(min)	10	10	10	10
Temperature (℃)	25	25	25	25

Table S2. 2θ Angle Values for Different Catalytic Surfaces

Catalyst	（111）	（200）	（220）
Commercial Pt/C	39.80°	-	-
Pt/SS	39.84°	46.44°	67.84°
PtNi/SS	40.34°	46.95°	68.50°
PtRu/SS	39.86°	46.48°	67.88°
PtRuNi/SS	40.30°	46.89°	68.48°

Table S3. The concentration of Pt, Ru and Ni in all samples by ICP-AES measurement.

Catalysis	Pt(mg/g)	Ru(mg/g)	Ni(mg/g)
Pt/SS	0.597	-	-
PtNi/SS	0.469	-	0.154
PtRu/SS	0.490	0.317	-
PtRuNi/SS	0.464	0.309	0.145

Table S4. Summary of MOR of the catalysts in the acid medium in recent literature.

Catalyst	solution	Mass Activity /A Mg^{-1}_{Pt}	ADT Current retention rate %	Reference
PtRuNi/SS	1 M MeOH + 0.5 M H_2SO_4	0.95	86.4	This work
$Pt_{60}Mn_{1.7}Co_{38.3}$/C	1 M MeOH + 0.5 M H_2SO_4	0.67	55	[12]
PtRu nanowires	0.1 M $HClO_4$ + 0.5 M CH_3OH	0.82	63.6	[13]
MWNT/2OH-PBi/Pt	0.1 M HClO4 + 1 M CH_3OH	1	50	[14]
Pt_1Cu_3	1 M MeOH + 0.5 M H_2SO_4	0.83	83.6	[15]
PtPb CNCs	0.1 M HClO4 + 1 M CH_3OH	0.97	68.7	[16]
GDY@PtCu	1 M MeOH + 0.5 M H_2SO_4	0.7	59	[17]
PtV ANNs/MWCNTs	0.5 M MeOH + 0.5 M H_2SO_4	0.71	65	[18]
$Cu_{0.3}Pt_3Sn$/CNTs	1 M MeOH + 0.5 M H_2SO_4	1.08	79	[19]
PtRu/C-TiN	0.5 M MeOH + 0.5 M H_2SO_4	0.81	61.1	[20]
PtPdCr/C	0.1 M $HClO_4$ + 0.5 M CH_3OH	0.96	58	[21]
$Pt_{47}Rh_8Cu_{45}$/C	0.1 M $HClO_4$ + 0.5 M CH_3OH	0.38	77	[22]
Ru–Pt_3Sn NC	0.1 M $HClO_4$ + 1 M CH_3OH	0.74	80	[23]

Table S5 The concentration of Pt, Ru and Ni in all samples by ICP-AES measurement.

Catalysis	Pt(mg/g)	Ru(mg/g)	Ni(mg/g)
Before ADT	0.464	0.309	0.145
After ADT	0.443	0.300	0.126

Table S6. Pt 4f Binding Energies for Different Catalysts (eV)

Catalyst	Pt^0	Pt^{2+}
Commercial Pt/C	71.91	73.10
Pt/SS	71.80	72.68
PtNi/SS	71.68	72.63
PtRu/SS	71.78	72.65
PtRuNi/SS	71.60	72.35

References

1. Kresse G, Furthmüller J. Efficiency of ab-initio total energy calculations for metals and semiconductors using a plane-wave basis set. *Comput. Mater. Sci.* 1996;6(1):15-50.

2. Kresse G, Hafner J. Ab initio molecular-dynamics simulation of the liquid-metal--amorphous-semiconductor transition in germanium. *Phys. Rev. B.* 1994;49(20):14251-14269.

3. Perdew JP, Burke K, Ernzerhof M. Generalized Gradient Approximation Made Simple. *Phys. Rev. Lett.* 1996;77(18):3865-3868.

4. Methfessel M, Paxton AT. High-precision sampling for Brillouin-zone integration in metals. *Phys. Rev. B.* 1989;40(6):3616-3621.

5. Grimme S. Semiempirical GGA-type density functional constructed with a long-range dispersion correction. *J. Comput. Chem.* 2006;27(15):1787-1799.

6. Mathew K, Sundararaman R, Letchworth-Weaver K, Arias TA, Hennig RG. Implicit solvation model for density-functional study of nanocrystal surfaces and reaction pathways. *J Chem Phys.* 2014;140(8):084106.

7. Poerwoprajitno AR, Gloag L, Watt J, et al. A single-Pt-atom-on-Ru-nanoparticle electrocatalyst for CO-resilient methanol oxidation. *Nat Catal.* 2022;5(3):231-237.

8. Sakong S, Groß A. The Importance of the Electrochemical Environment in the Electro-Oxidation of Methanol on Pt(111). *ACS Catal.* 2016;6(8):5575-5586.

9. Yoo JS, Abild-Pedersen F, Nørskov JK, Studt F. Theoretical Analysis of Transition-Metal Catalysts for Formic Acid Decomposition. *ACS Catal.* 2014;4(4):1226-1233.

10. Zuluaga S, Stolbov S. Factors controlling the energetics of the oxygen reduction reaction on the Pd-Co electro-catalysts: Insight from first principles. *J. Chem. Phys.* 2011;135(13):134702.

11. Wang V, Xu N, Liu J-C, Tang G, Geng W-T. VASPKIT: A user-friendly interface facilitating high-throughput computing and analysis using VASP code. *Comput. Phys. Commun.* 2021;267:108033.

12. Deshpande P, Prasad BLV. Alloying with Mn Enhances the Activity and Durability of the CoPt Catalyst toward the Methanol Oxidation Reaction. *ACS Appl Mater Interfaces.* 2023;15(22):26554-26562.

13. Huang L, Zhang XP, Wang QQ, Han YJ, Fang YX, Dong SJ. Shape-Control of Pt-Ru Nanocrystals: Tuning Surface Structure for Enhanced Electrocatalytic Methanol Oxidation. *J. Am. Chem. Soc.* 2018;140(3):1142-1147.

14. Yang ZH, Luo F. Pt nanoparticles deposited on dihydroxy-polybenzimidazole wrapped carbon nanotubes shows a remarkable durability in methanol electro-oxidation. *Int J Hydrogen Energy.* 2017;42(1):507-514.

15. Lu L, Chen S, Thota S, et al. Composition Controllable Synthesis of PtCu Nanodendrites with Efficient Electrocatalytic Activity for Methanol Oxidation Induced by High Index Surface and Electronic Interaction. *The Journal of Physical Chemistry C.* 2017;121(36):19796-19806.

16. Huang L, Zhang XP, Hang YJ, Wang QQ, Fang YX, Dong SJ. High-Index Facets

Bounded Platinum-Lead Concave Nanocubes with Enhanced Electrocatalytic Properties. *CHEMISTRY OF MATERIALS.* 2017;29(10):4557-4562.
17. Pan HH, Jiang ZQ, Zuo ZC, et al. Proton selective anode nanochannel for efficient methanol utilization. *NANO TODAY.* 2021;39:No.101213.
18. Zhang JM, He JJ, Wang XQ, et al. One-step synthesis in deep eutectic solvents of PtV alloy nanonetworks on carbon nanotubes with enhanced methanol electrooxidation performance. *Int J Hydrogen Energy.* 2019;44(54):28709-28719.
19. Nie Y, Li ZH, Wang Y, et al. The 5d-5p-3d orbital hybridization induced by light incorporation of Cu into surface-uneven Pt3Sn intermetallic nanocubes customizes dual-intermediates adsorptions for CO-resilient methanol oxidation. *Applied Catalysis B-Environ.* 2024;343: No.123494.
20. Sui XL, Li CZ, Zhao L, Wang ZB, Gu DM, Huang GS. Mesoporous g-C_3N_4 derived nano-titanium nitride modified carbon black as ultra-fine PtRu catalyst support for Methanol electro-oxidation. *Int J Hydrogen Energy.* 2018;43(10):5153-5162.
21. Peng K, Bhuvanendran N, Ravichandran S, et al. Carbon supported PtPdCr ternary alloy nanoparticles with enhanced electrocatalytic activity and durability for methanol oxidation reaction. *Int J Hydrogen Energy.* 2020;45(43):22752-22760.
22. Sun B, Huang L, Su S, et al. PtRhCu ternary alloy nanodendrites with enhanced catalytic activity and durability toward methanol electro-oxidation. *Mater. Chem. Phys.* 2020;252 No.123234.
23. Yang TY, Qin FJ, Zhang SP, Rong HP, Chen WX, Zhang JT. Atomically dispersed Ru in Pt_3Sn intermetallic alloy as an efficient methanol oxidation electrocatalyst. *Chem Commun.* 2021;57(17):2164-2167.